SOLAR THERMAL REACTOR MATERIALS CHARACTERIZATION

Paul R. Lichty[1], Amanada M. Scott[2], Christopher M. Perkins[1], Carl Bingham[3], * Alan W. Weimer[1].

(1) Department of Chemical and Biological Engineering, University of Colorado. (2) Department of Chemical Engineering, Vanderbilt University. (3) National Renewable Energy Lab(NREL).

1111 Engineering Dr. UCB 424, Boulder, CO 80309 USA. (303) 492-1340
Paul.Lichty@colorado.edu

Abstract:

Current research into hydrogen production through high temperature metal oxide water splitting cycles has created a need for robust high temperature materials. Such cycles are further enhanced by the use of concentrated solar energy as a power source. However, samples subjected to concentrated solar radiation exhibited lifetimes much shorter than expected. Characterization of the power and flux distributions representative of the High Flux Solar Furnace(HFSF) at the National Renewable Energy Laboratory(NREL) were compared to ray trace modeling of the facility. In addition, samples of candidate reactor materials were thermally cycled at the HFSF and tensile failure testing was performed to quantify material degradation. Thermal cycling tests have been completed on super alloy Haynes 214 samples and results indicate that maximum temperature plays a significant role in reduction of strength. The number of cycles was too small to establish long term failure trends for this material due to the high ductility of the material.

Keywords: Concentrated Solar, Solar Materials, Thermal Shock

1 Introduction:

1.1 Motivations:

The increasingly apparent need for clean renewable energy sources has helped to spurned research in solar driven processes. Through photovoltaic, trough, and high concentration solar, many researchers understand the benefit of deriving energy directly from the sun. New innovations are pushing the limits of material tolerances and lifetimes. Characterizing typical temperature and stress values associated with solar testing can greatly assist in the search for usable materials.

Solar hydrogen production, via thermo-chemical metal oxide water splitting cycles, presents an application in which robust high temperature materials are needed [1]. The unique temperature profiles and stress distributions for the facility must be quantified to more easily identify candidate materials. Dahl et. al. have shown the feasibility of driving chemical cycles in aerosol flow reactors using concentrated solar energy [2]. In their experiments at the HFSF concentrated solar energy was used to drive a methane cracking reaction. The reactor consisted of an outer quartz tube and inner reaction containing tube. The Quartz tube was sealed to the environment and purged with an inert gas to protect the inner tube from oxidation. The tubes were received and sealed from one another by the cooling chambers at the top and bottom of the apparatus. Process gas and particles were feed down the inner tube and reacted at high temperatures (~2000K). The reactor used in these experiments can be seen in Figure 1.

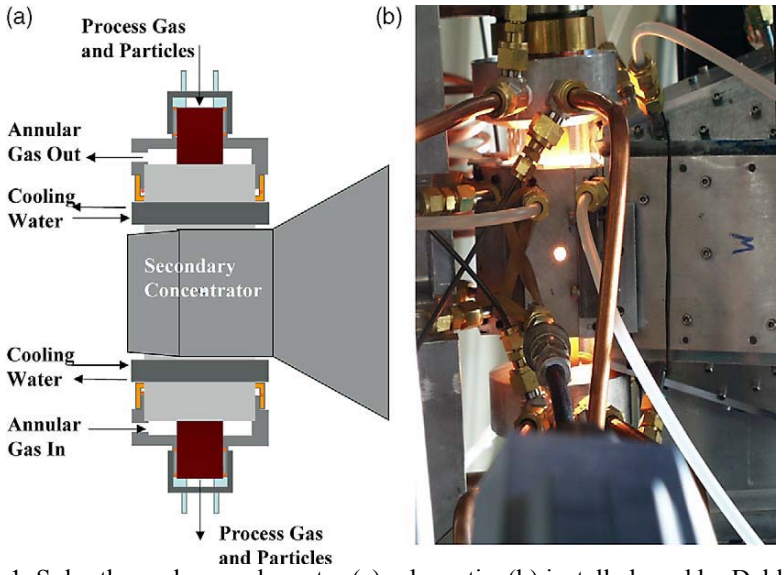

Figure 1. Solar thermal aerosol reactor (a) schematic, (b) installed used by Dahl et. al.

Because the methane dissociation reaction did not involve any oxygen graphite tubes were used because of their superior high temperature and thermal shock stability. Due to the creation of oxygen during the dissociation step of metal oxide reactions (e.g. ZnO, Mn_2O_3, Fe_3O_4), tube materials must be oxidation resistant. Several candidate materials, such as Alumina and Silicon Carbide, have undergone preliminary testing at the HFSF. The unpublished results of these tests showed that samples subjected to the intense solar radiation cycling exhibited lifetimes much shorter than expected. The primary failure mechanism was radial fracture. It is believed that this failure is due in part to the large temperature gradient across the tube surface. This gradient is a function of the slow heat conduction within the materials and the unique thermal profile created by the incident solar energy. The motivation of this research is to couple the solar characteristics of the HFSF with the stresses induced in the test materials to more easily select usable solar materials.

1.2 Concentrated Solar Energy:

Concentrated solar energy focuses large areas of sunlight onto a very small point using concave mirrors or lenses. Peak concentrations at the HFSF using a secondary concentrator reach 2500 W/m^2, with maximum theoretical power up to 10 kW. This type of solar application produces unique flux profiles that create drastic thermal gradients within sample materials. Lewandowski et. al originally characterized the HFSF by measuring the power profile using seven horizontal 2.5cm diameter calorimeters[3]. The flux intensity was measured as a function of position along the focal axis. These test were performed for the beam produced by the primary concentrator and then again for a round compound parabolic concentrator. In addition flux profiles were measured using BEAMCODE analysis software. A similar approach has been attempted to characterize the HFSF with the octagonal secondary concentrator used by Dahl et. al. for the solar thermal aerosol reactor.

The secondary is composed of eight mirrors attached at compound angles to produce a cone with a rectangular exit. The mirrored surface was achieved by coating the internal face of the pieces with protected silver. Recent measurements of the reflectance of the secondary show an average reflectance of 96 percent. A picture of the secondary assembly can be seen in Figure 2. The flux profile of the incident solar radiation at the exit of the secondary is pertinent to accurately modeling the conditions seen by the reaction containing tube.

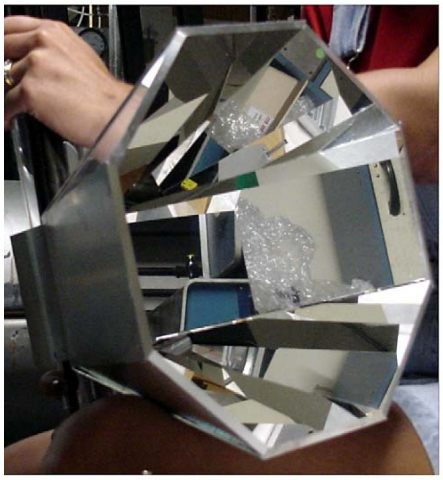

Figure 2. Secondary Concentrator

Through power and flux profile measurements we can more accurately describe the internal stresses produced within reactor materials. Predicting and understanding the thermo-elastic stresses inherent to concentrated solar energy applications is imperative for usable materials characterization and technology scale up.

1.3 Failure Mechanism:

Ceramic materials best suited for high temperature oxidizing environments are often very brittle thus causing poor thermal shock resistance. Because of the rapid temperature fluctuations that can accompany concentrated solar testing usable materials must be capable of withstanding large thermo-mechanical stresses caused by temperature variations and gradients. There has been a significant amount of research directed towards understanding and describing the internal stresses that arise during temperature fluctuation[3-10].

Thermal shock describes the creation of stress due to rapid temperature variations. Because solar facilities are dependant on weather conditions the most common cause of rapid temperature variation is shading due to cloud cover. Many papers have been published pertaining to the occurrence of thermal shock degradation specifically in ceramic materials. A common test method of determining the thermal shock characteristics of materials is the "quench method"[11]. This involves slow heating of materials to a prescribed temperature followed by rapid quenching into a medium held at a cooler temperature[12]. The residual strength of the materials can be measured through failure testing. The critical failure temperature difference(ΔT_c) can be found by performing these tests at varying temperature differences. However, the rate of temperature change is difficult to determine. In water the hot materials create a steam envelope which inhibits heat transfer[13]. Therefore, some researchers have conducted tests in which air jets are used to control the rate of cooling[14]. This method also allows the sample to be, more easily cycled.

For thermal shock that occurs at temperature differences below ΔT_c materials are still subject to stresses that can cause failure after repeated cycling. Thermal stress σ_H is calculated using eqn. 1:

$$\sigma_H = \frac{E\alpha\Delta T}{1-\nu}$$

Where E is Young's modulus, α is thermal expansion coefficient, ΔT is the temperature change, and ν is the Poissons's ratio of the material[12]. It is useful to determine the expected ΔT's that occur at the solar furnace due to cloud shading so that we may establish a stress history specific to the HFSF. Materials must be capable of withstanding the thermal cycling that would accompany a large scale concentrated solar facility.

2 Methods:

2.1 Furnace Characterization:

For the purpose of this research the power, flux profile, and heating/cooling rate measurements were the significant variables that were tested. For the power measurements a black body absorber was placed at the exit of the secondary. The absorber was water cooled and power was measured from the mass flow rate, $\dot{m}$, and the change in temperature, ΔT, using the equation $Q = \dot{m}Cp\Delta T$ [15]. The temperature of the water at the entrance and exit of the absorber was measured using 4-wire 100-ohm platinum resistance temperature detectors. The water flow rate was measured using a Flow Technologies FT 6-8 turbine flowmeter with amplifier and D-A converter for analog output. Power measurements were made at varying water flow rates to reduce calibration error from the mass flow controller. Also, the aperture opening was varied in order to accurately predict the power during heat up and cool down and these values were normalized for normal incident power(NIP) measurements.

Flux profile measurements were obtained using BeamView software from Coherent. A piece of frosted quartz was placed at the exit of the secondary and a Coherent LaserCam IIID Camera was used to capture the light intensity profile. This profile data was coupled with the power data to obtain an equation that describes the flux at the exit of the secondary.

2.2 Modeling

Soltrace was used to model the HFSF and secondary. Soltrace is a ray tracing program developed by NREL. The program is specifically tailored to study solar systems. Solar rays coming from the sun are discretized into individual vector elements. These vectors interact with optical elements placed on a global coordinate system. A description of the ray-tracing procedure used is given by Spencer et al.

2.3 Thermal Cycling

Tensile testing samples of Haynes 214 were fabricated according to ASTM E8 – 04. The samples had an overall length of .232m with a gauge thickness of .0017m and gauge length of .05m[16]. These samples were annealed and oxidized in a horizontal tube furnace at 1100 C for two hours to form a uniform alumina oxide layer[17]. A mounting rack was constructed behind the secondary concentrator and samples were positioned .0635m behind the exit of the secondary, the same position as the reaction containing tubes in the Dahl reactor. This configuration can be seen in Figure 3. Sample temperatures were monitored by a pyrometer focused on the rear of the samples. The pyrometer was made by Heitronics, model KT 19.01. Samples were slowly heated to the desired temperature and held for two minutes in order to attain a constant temperature. To simulate cloud interference guillotine style shutters were closed and the sample was allowed to cool. Because the thermal shock values attainable by this method are less than the ΔT_c of the material the samples were thermally cycled to determine material degradation. The experimental matrix was created for three factors; maximum power level, cycle time, and number of cycles. The first two control variables correspond to the maximum temperature, ΔT amplitude respectively. Maximum power was controlled by an automatic aperture, the power levels tested were 2000 and 2500W. These power levels correspond to approximate temperatures of 1200 and 1300 C respectively. To accommodate changes in the NIP the aperture was looped to a control based on equations obtained from our power measurements. Closed and opened cycle times of 20s-35s, and 40s-40s respectively, correspond to ΔT's of approximately 500 and 700 °C. Cycle levels were 20, 30, and 40 cycles. The experimental design was a 2^3 factorial with a center point in the cycle factor to determine curvature. Each point of this factorial design was performed twice and the order was randomized.

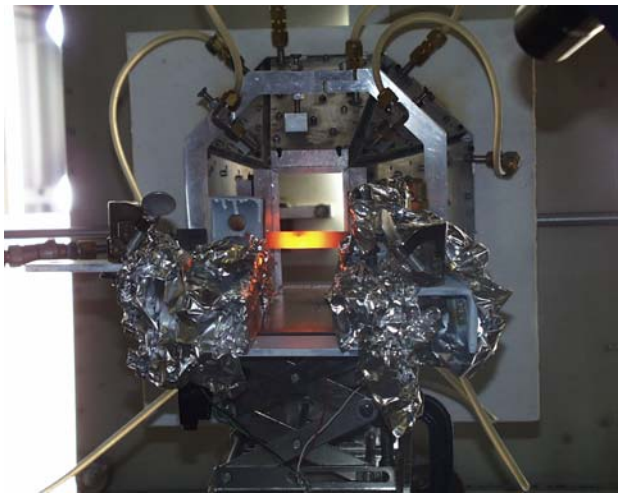

Figure 3. Material sample on cooling phase of temperature cycle.

The residual strength of the cycled samples was then obtained through tensile testing according to ASTM E8 – 04. The samples were tested using an Instron 5869 Universal Testing Machine with a 50kN maximum capacity. All samples were tested with a constant rate of head separation of .0001 m/s. Cycled samples were compared with control samples to determine extent of degradation. Ultimate stress was used as the response variable for statistical analysis.

3 Results:

3.1 Solar Furnace Characterization

The surface plot for the furnace power as a function of the NIP and the shutter attenuation can be seen in Figure 4. The equation derived form this regression was used to maintain consistent power on the sample as the NIP changed throughout the day. The equation is as follows:

$$Power = 25856 + 146 * (\%Attenuation) - 66 * (NIP) - .062 * (\%Attenuation)^2 + .04 * (NIP)^2$$

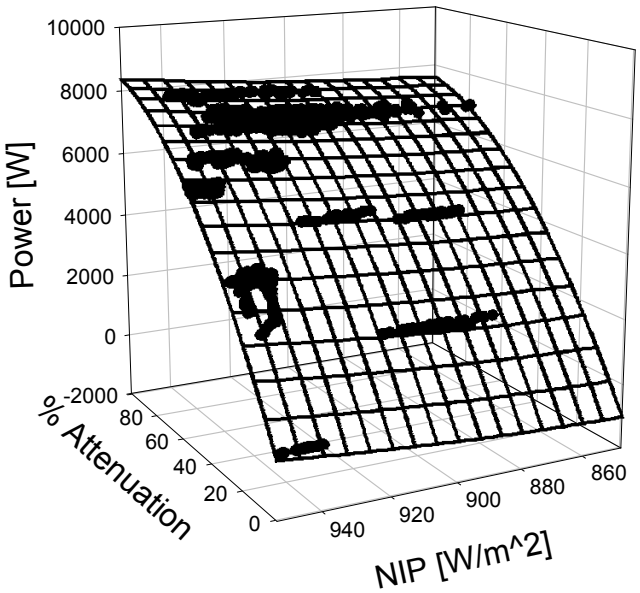

Figure 4. Power as a function of NIP and percent shutter attenuation.

Flux profiles have been obtained from modeling and experimental methods described above. However, the discrepancies between the data are very large. These discrepancies are significant along the outer edges of the plots. Further experimentation and analysis is required to mitigate the differences.

3.2 Haynes 214 Cycling

Thermal stress values for the Haynes 214 samples were obtained using the temperature curves measured from the pyrometer. In the thermal shock literature the temperature change (ΔT) is considered to occur instantaneously. Because of the time dependant heating and cooling rates of these experiments the ΔT's used were taken over a one second interval. Typical values of the maximum and minimum thermal stresses achieved through these tests can be seen in Table 1. Negative values correspond to tensile stress occurring during cooling and positive values correspond to compressive stress which occurs during heating.

Power [W]	Cycle [s]	σ_{MAX} Tensile [Mpa]	σ_{MAX} Compression [Mpa]
2000	20-35	-282	251
2000	40-40	-311	361
2500	20-35	-348	361
2500	40-40	-365	432

Table 1. Maximum cyclic stress

Typical ultimate tensile strength of cold-rolled solution annealed Haynes 214, at room temperature, is 995 MPa with typical 0.2% offset yield strength of 605 MPa [18]. The thermal stresses produced during testing are below those needed to fracture or deform the samples. Plots of the stress and temperature as a function of time can be seen in figure 5. Larger stresses occur with higher power levels and cycle times.

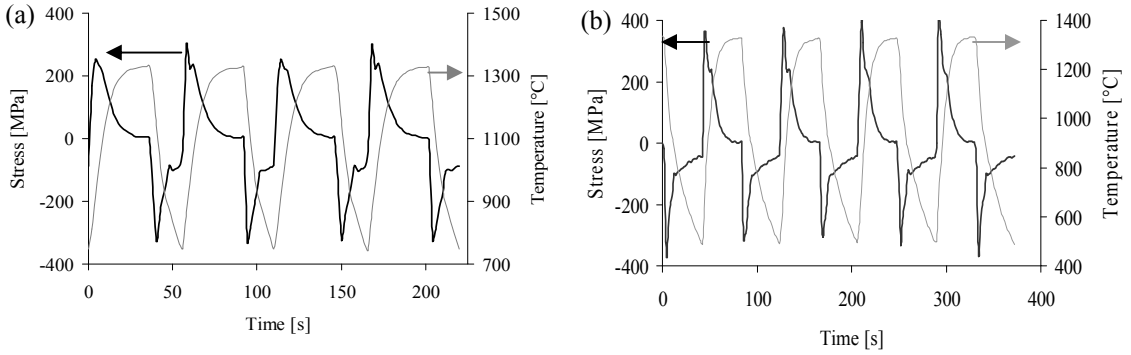

Figure 5. (a) 2500W, 20-35s cycles, (b) 2500W, 40-40s cycles.

Analysis of the Ultimate stress response for the factorial design can show that the power level is the only variable that is significant within 95% confidence. The average Ultimate stress for the control samples was found to be 948.2 ± 3.4 MPa. The average residual ultimate stress and percent deviation from the control can be seen in Table 2. While the number of cycles plays no significant role a trend can be seen in Figure 6 that may indicate further cycling is needed to have an effect.

Power	Avg. Ultimate stress [Mpa]	%deviation
2500	873.0 ± 30.2	7.9
2000	902.1 ± 37.5	4.9

Table 2. Residual Ultimate stress and deviation from control.

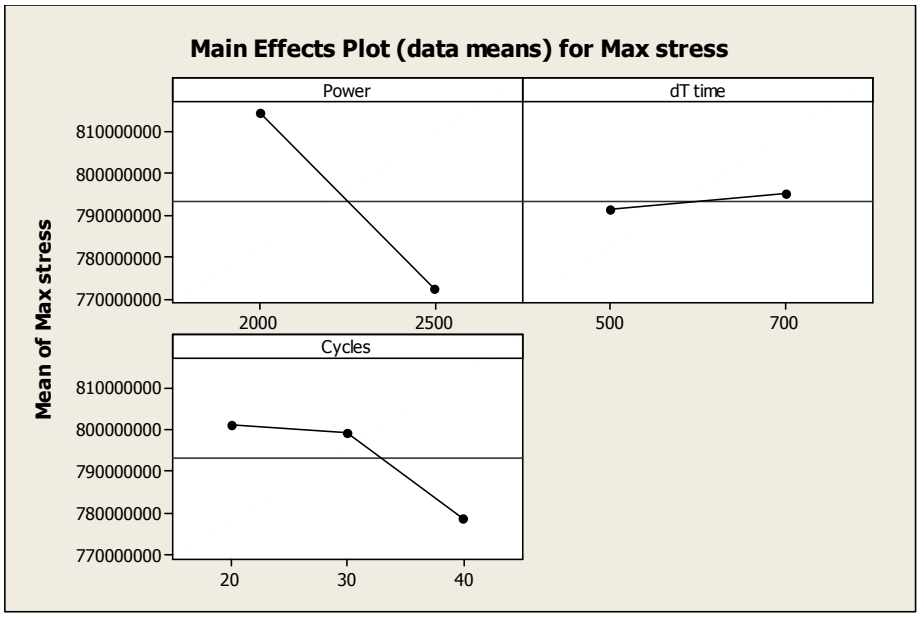

Figure 6. Normalized plot of the main effect.

4 Discussion:

Characterization of the HFSF at NREL has been performed. A power control equation has been found to ensure consistent power levels on samples. Consistent peak temperatures during cycling tests confirm the reliability of the control equation. Exit flux profiles have been found through experimentation and ray trace modeling. Unfortunately these plots have large discrepancies especially toward the outer edges of the surface. Further testing is required to detect the cause of the disparity and create a better correlation between experimental and modeled flux profiles.

Cyclic thermal tests have been performed on super alloy Haynes 214. The results of these tests show that maximum temperature is the only factor that plays a significant role in reduction of residual ultimate strength. The number of cycles had to be limited in order to make testing time reasonable. The stress history corresponding to solar testing can now be repeated in lab to get accurate lifetime predictions. Further testing of ceramic samples is planned. These materials can with stand higher temperatures but are more susceptible to thermal shock damage.

5 Acknowledgements:

The author would like to acknowledge the significant contributions made by Allan Lewandowski toward modeling of the solar facility. Funding was provided through the Department of Energy solar thermochemical hydrogen production (STCH) program.

6 References:

1. Perkins C, Weimer A. Likely near-term solar-thermal water splitting technologies. International Journal of Hydrogen Energy 29 **15** (2004) 1587-1599.

2. Dahl J, Buechler K, Finley R, Stanislaus T, Weimer A, Lewandowski A, Bingham C, Smeets A, Schneider A. “Rapid solar-thermal dissociation of natural gas in an aerosol flow reactor.” Energy, Volume 29, Issues 5-6, April-May 2004, Pages 715-725

3. Lewandowski, A., C. Bingham, et al. (1991). "Performance Characterization of the Seri High-Flux Solar Furnace." Solar Energy Materials **24**(1-4): 550-563.

4. Akiyama, S. and S. Amada (1992). "Estimation of Fracture Conditions of Ceramics by Thermal-Shock with Laser-Beams Based on the Maximum Compressive Stress Criterion." Jsme International Journal Series I-Solid Mechanics Strength of Materials **35**(1): 91-94.

5. Akiyama, S. and S. Amada (2001). "Thermal shock strength of Al2O3 by laser irradiation method." Ceramics International **27**(2): 171-177.

6. Kovalenko, A. D. (1969). Thermoelasticity Basic Theory and Applications. The Netherlands, Wolters-Noordhoff Publishing Groningen.

7. Lessen, M. (1956). "Thermoelasticity and Thermal Shock." Journal of the Mechanics and Physics of Solids **5**(1): 57-61.

8. Segall, A. E. (2003). "Thermal stresses in an infinite slab under an arbitrary thermal shock." Journal of Applied Mechanics-Transactions of the Asme **70**(5): 779-782.

9. Tomba, A. G. and A. L. Cavalieri (2000). "Alumina disks with different surface finish: thermal shock behavior." Journal of the European Ceramic Society **20**(7): 889-893.

10. Tomba, A. G. and A. L. Cavalieri (2000). "Evaluation of the heat transfer coefficient in thermal shock of alumina disks." Materials Science and Engineering a-Structural Materials Properties Microstructure and Processing **276**(1-2): 76-82.

11. Becher, P. F., D. Lewis, et al. (1980). "Thermal-Shock Resistance of Ceramics - Size and Geometry-Effects in Quench Tests." American Ceramic Society Bulletin **59**(5): 542-&.

12. Collin, M. and D. Rowcliffe (2000). "Analysis and prediction of thermal shock in brittle materials." Acta Materialia **48**(8): 1655-1665.

13. Lewis, D. (1981). "The Water Quench Thermal-Shock Test - a Summary Analysis." American Ceramic Society Bulletin **60**(3): 383-383.

14. Hugot, F. and J. C. Glandus (2007). "Thermal shock of alumina by compressed air cooling." Journal of the European Ceramic Society **27**(4): 1919-1925.

15. Howell, R. S. a. J. (2002). Thermal Radiation Heat Transfer 4Th Edition, Taylor & Francis.

16. ASTM standard E8 – 04.

17. Rao, K.V., Herchenroeder R. B. Microstructural Characteristics of Haynes alloy no. 214, A New Superalloy Developed For Applications In Hostile, High-Temperature Environments.

18. Haynes International, Product catalog for Haynes 214, downloaded from http://www.haynesintl.com/ on 5/23/07.